ISSN 0036-0236, Russian Journal of Inorganic Chemistry, 2024, Vol. 69, No. 3, pp. 394–406. © Pleiades Publishing, Ltd., 2024.

PHASE EQUILIBIRA IN INORGANIC SYSTEMS: THERMODYNAMICS AND MODELING

Modeling of Phase Equilibria in the La_2O_3–SrO–ZrO_2 System Using the NUCLEA Database

V. A. ~~Vorozhtsov~~[a], *, V. I. ~~Al'myashev~~[a, b], and V. L. Stolyarova[a, c]

[a] *Grebenshchikov Institute of Silicate Chemistry, Russian Academy of Sciences, St. Petersburg, 199034 Russia*

[b] *~~Aleksandrov~~ Research Institute of Technology, Sosnovyi Bor, 188540 Russia*

[c] *St. Petersburg State University, St. Petersburg, 199034 Russia*

**e-mail: v.vorozhcov@rambler.ru*

Received September 15, 2023; revised October 16, 2023; accepted October 23, 2023

Abstract—The goal of this work was to study phase equilibria in the La_2O_3–SrO–ZrO_2 system, which is a promising base for high-temperature ceramics and materials with unique optical, electrochemical, and catalytic properties. Thermodynamic modeling of phase equilibria in this system was carried out using the NUCLEA database and GEMINI2 (Gibbs Energy Minimizer) software. One polythermal and thirteen isothermal sections of the La_2O_3–SrO–ZrO_2 phase diagram were calculated in the temperature range 600–3023 K. The ~~thus gained~~ data on La_2O_3–SrO–ZrO_2 phase equilibria were discussed with reference to information available on the ~~component~~ binary systems. The modeled phase relations in the ternary system under study correlate completely with the phases existing in the ~~component~~ binary systems. The temperature evolution of the phase relations and boundaries of single-phase, two-phase, and three-phase areas in the system were considered. Four ternary eutectic points were identified at 2039 K, 2105 K, 2120 K, and 2351 K.

Keywords: phase equilibria, composition–temperature diagrams, CALPHAD, thermodynamic modeling, NUCLEA database

DOI: 10.1134/S0036023623602957

INTRODUCTION

The La_2O_3–SrO–ZrO_2 system is part of multicomponent systems on the basis of which high-entropy complex oxides with a perovskite structure can be prepared [1–3]. Having widely variable chemical compositions, such compounds have a unique combination of physical and chemical properties, such as high-temperature stability, chemical ~~durability~~, and promising optical, electrochemical, magnetic and catalytic characteristics [3]. It is for this reason that high-entropy perovskite oxide systems are offered numerous areas of application. For example, multicomponent perovskites containing lanthanum and strontium were considered as thermal barrier coatings [4], oxygen carriers in catalytic chemical looping reforming [5, 6], oxygen storage and transport materials [7], high-temperature proton conductors [8], electrode materials [9] for solid oxide fuel cells [10] and anodes in lithium-ion batteries [11].

For the successful synthesis and application of these materials, information is needed on phase equilibria in systems on which materials design is based. However, an ~~increment~~ in the number of components adds much difficulty to an experimental study of a multicomponent phase diagram. In this regard, of particular relevance is an option to calculate phase equilibria in a multicomponent system based on detailed data on binary systems and ~~individual~~ information on phase relations in a multicomponent system. There is no doubt that modeling of multicomponent phase diagrams is impossible without a preliminary research and optimization of phase equilibria in systems with a smaller number of components. This makes relevant calculations of phase equilibria in the La_2O_3–SrO–ZrO_2 system as part of multicomponent oxide systems~~, which~~ are of significant interest for materials design. It must be emphasized that we have not retrieved any piece of information in the literature on the La_2O_3–SrO–ZrO_2 ternary phase diagram, while the relevant binary systems have been studied. Available data on phase relations in the La_2O_3–SrO, La_2O_3–ZrO_2 and SrO–ZrO_2 binary systems will be briefly discussed below in the Section "Calculation Methods".

There is a wide variety of methods for calculating multicomponent phase equilibria, as shown, for example, by Shestakov and Grachev [12]. It should be mentioned that authors of this work participated in the development of a semiempirical method for calculating liquidus temperatures in multicomponent systems based on the liquidus temperatures in the ~~component~~ binary systems [13]. The geometric method for assembling ~~spatial~~ computer models of isobaric phase dia-

grams from surfaces and phase areas deserves special mention [14–17]. The advantage of this approach is its ability to take into account all topological features of the phase diagram, including predictions of all possible invariant phase transformations, based on scarce available information about phase relations in, e.g., component binary systems and primary crystallization surfaces in the multicomponent system [14] using the Gibbs phase rule and the Palatnik–Landau contact rule of phase regions [18]. The assembly of computer models of phase diagrams enables one to reliably interpret and resolve contradictions in experimental phase equilibria data by a reasoned selection of the most correct information or by design of several versions of the phase diagram [17, 19].

Currently, the most common approach for calculations of phase equilibria is CALPHAD (CALculation of PHAse Diagrams) [20, 21]. CALPHAD makes it possible to develop a unified and consistent model for the physicochemical description of the system based on all available information on phase relations, thermodynamic properties, and other characteristics (magnetism, electrical conductivity). The resulting model should contain optimized concentration and temperature dependences of the Gibbs energy and their derivatives for all phases of the system under study, to be used in modeling phase transformations, microstructure evolution, energies of metastable states, viscosity, and diffusion in multicomponent materials [21].

For the CALPHAD method to operate successfully, it is necessary to use special thermodynamic databases and models that describe the various thermodynamic functions of systems in accordance with experimental values. The development of thermodynamic databases and models has required significant efforts of large research groups, as a result of which the ThermoCalc [22], MTData [23], FactSage [24], and NUCLEA [25, 26] software packages were created. In recent years, the Atomic Energy Agency of the Organization for Economic Cooperation and Development has been working to create the most modern thermodynamic database, namely TAF-ID (Thermodynamics of Advanced nuclear Fuels—International Database), designed to solve nuclear energy problems and eliminate deficiencies identified over four decades of using existing databases [27]. Even in the most developed databases, however, experimental information on phase equilibria and thermodynamic properties gathered by Russian research groups over the past few decades is represented to an insufficient extent. Experimental data on the thermodynamic properties of inorganic systems determined in Russia by high-temperature mass spectrometry [28] over the past forty years, is only 10% included in international databases, and for hafnium oxide systems, for example, it is not mentioned at all. These facts indicate the need to create a National Thermodynamic Database for calculating phase equilibria of multicomponent systems and materials at high temperatures, taking into account the unique information accumulated recently by Russian scientists. The implementation of this idea will require the development of independent software and a new optimization of the entire array of available data using advanced models.

Therefore, the goal of this work was to study phase equilibria in the La_2O_3–SrO–ZrO_2 system in terms of the CALPHAD approach using the NUCLEA database. The tasks to be fulfilled included: the calculation of selected isothermal sections of the phase diagram of the system under consideration, in order to enable us to trace how phase relations in the system change with increasing temperature; calculation of the $La_2Zr_2O_7$–$SrZrO_3$ polythermal section between the compounds of greatest practical relevance; and consideration of the results of calculations with reference to extant data on phase equilibria in the component binary systems.

CALCULATION METHODS

Phase equilibria in the La_2O_3–SrO–ZrO_2 system were calculated using the NUCLEA database and GEMINI2 (Gibbs Energy MINImizer) software [25, 26]. The NUCLEA database was designed for calculations of phase equilibria and the thermodynamic description of systems of interest for the analysis of accident scenarios at nuclear reactors. Subsequently, however, this database has proven itself to solve a wider range of problems and has been successfully used for considering phase relations in various multicomponent systems [25, 29]. The software has been used to calculate isothermal and polythermal sections of phase diagrams for the Al_2O_3–SiO_2–ZrO_2 [19, 30] and Zr–C–O [31] systems; the authors of this paper participated in that work.

The NUCLEA database [25, 26] is based on the optimization of experimental data on phase equilibria and thermodynamic properties gathered in more than 300 binary and ternary systems. The database stores this information in the form of concentration and temperature dependences of the Gibbs energy of all studied phases. In order to calculate phase equilibria, one has to minimize the total Gibbs energy of the system using the GEMINI2 calculation module. The total Gibbs energy of the system is considered in relation to the selected standard states of the basic components of the system, and is calculated as the sum of the Gibbs energies of individual phases, also referred to the standard states of the basic components. Stoichiometric compounds, ideal gas mixtures, and condensed solutions are distinguished among the phases. When calculating the Gibbs energy of a compound referred to the standard state of the compound, one considers the Gibbs energy of formation of the compound from its basic components in the standard states at set conditions, and takes into account the Gibbs energies of conversion of the basic components from their stationary states to the forms in which they exist in the

compound (lattice stabilities). The temperature-dependent Gibbs energies of compounds and transformations of basic components are described by an equation that includes the powers of the variable temperature from minus ninth to seventh, the natural logarithm of temperature, and the product of temperature by its natural logarithm.

To model the thermodynamic properties of condensed solutions, a generalized lattice model with an option to introduce several sublattices (a sublattice model) is used [32]. The Gibbs energy of a condensed solution consists of the Gibbs energies of standard substances, Gibbs energy of ideal mixing, excess Gibbs energy, and in some cases, energies of magnetism and ordering. Standard substances are recognized by considering all possible permutations in the various sublattices and then assuming that each sublattice is completely filled with only one component. The Gibbs energy of ideal mixing is determined through the atomic fractions of components in the sublattices. The excess Gibbs energy is related to the interaction parameters of the components, which depend on the composition according to the Redlich–Kister polynomial [33] in the case of binary interactions and as a first-order polynomial of the component atomic fractions in the sublattice in the case of triple interactions. The specific expressions used for the concentration-dependent excess Gibbs energy and interaction parameters depend on the number of sublattices in the model. In general, up to four model sublattices can be used to describe the excess Gibbs energy of a solution, but the parameters of triple interactions are taken into account only for one- and two-sublattice models.

The GEMINI2 allows you to extrapolate the thermodynamic description available in the database to systems that were not taken into account when the software was developed. In this way, it is possible to calculate phase equilibria for a wide range of systems containing phases comprising twenty elements, including lanthanum, strontium, oxygen, and zirconium necessary for this work. However, NUCLEA is a closed database; that is, it does not allow users to make changes and additions. One consequence is the impossibility to calculate phase equilibria in systems that contain chemical elements other than those twenty elements taken into account in the database. In addition, it makes a problem to update the initial data set for calculations, especially when new, more reliable experimental results appear covering wider temperature ranges.

For the correct interpretation of the phase equilibria in the La_2O_3–SrO–ZrO_2 system calculated here, we will consider available information on phase diagrams of La_2O_3–SrO, La_2O_3–ZrO_2 and SrO–ZrO_2 binary systems.

The La_2O_3–SrO phase diagram has been studied in several works, summarized by Lopato [34] and by Grundy et al. [35] (Fig. 1). No intermediate compounds were noticed in the system at 1173 [36] and 1373 K [37, 38]. Schulze and Müller-Buschbaum [39] identified the intermediate compound $La_4Sr_3O_9$ within the narrow temperature range 2133–2173 K. Huang et al. [40] prepared a La_4SrO_7 phase by solid-phase technology with anneals at temperatures above 1673 K, and mentioned that they had not checked whether this phase had a homogeneity area, but failed to prepare the compound $La_2Sr_2O_5$. According to Lopato [34] and Grundy et al. [35], two compounds exist in the La_2O_3–SrO system: $La_4Sr_3O_9$ with a zero homogeneity extent and a nonstoichiometric compound, called the β phase, containing ca. 25–35 mol % strontium oxide. $La_4Sr_3O_9$ is stable at temperatures above 1773 K [34] or 1737 K [35] and melts incongruently at 2133 K [34, 35]. The β phase is stable at temperatures above 1813 K [34] or 1850 K [35] and melts congruently at 2373 K [34, 35]. The phases corresponding to the terminal oxides dissolved the second component: a higher solubility of SrO in La_2O_3 (more than 20 mol % SrO) against less than 5 mol % La_2O_3 in SrO. Two eutectic points were found in the La_2O_3–SrO system: the crystallization of La_2O_3 and the β phase at 2253 K and 27 mol % SrO [34] or at 2363 K and 25 mol % SrO [35], and the crystallization of $La_4Sr_3O_9$ and the β phase at 2103 K and 55 mol % SrO [34] or 53 mol % SrO [35]. Thus, the greatest contradiction is with the La_2O_3 + β phase → L (L stands for melt) eutectic, the temperature of which in published works is differentiated by more than 100 K.

The NUCLEA database uses only Lopato's phase equilibria data [34] in the optimization of the La_2O_3–SrO phase diagram. However, as Fig. 1 shows, the optimized phase equilibria in the NUCLEA database slightly differ from the documented results referred to above. Both compounds of the system are considered as having no homogeneity extents; the β phase is formulated as La_4SrO_7. $La_4Sr_3O_9$ is stable at temperatures above 1777 K and melts incongruently at 2131 K. La_4SrO_7 is stable in the temperature range 1814–2370 K, above which it melts congruently. SrO is also considered as a compound of constant composition, and La_2O_3 can dissolve up to 21 mol % SrO. In addition, La_2O_3 polymorphism is not taken into account; instead, the only cubic polymorph of lanthanum oxide is considered at all temperatures until melting. Eutectics have the coordinates 2349 K and 28.9 mol % SrO for La_2O_3 and La_4SrO_7 solidification, and 2096 K and 51.4 mol % SrO La_4SrO_7 and $La_4Sr_3O_9$ solidification. Therefore, the La_2O_3 + La_4SrO_7 → L eutectic temperature (2349 K) in NUCLEA is closer to Grundy et al.'s results [35] (2363 K) than to Lopato's [34] (2253 K), while the eutectic composition (28.9 mol % SrO), on the contrary, is closer to Lopato's [34] value (27 mol % SrO). When considering data that were calculated using the NUCLEA database, it is advisable to be cautious about the results of modeling phase equilibria involving La_4SrO_7 and SrO; the database treats

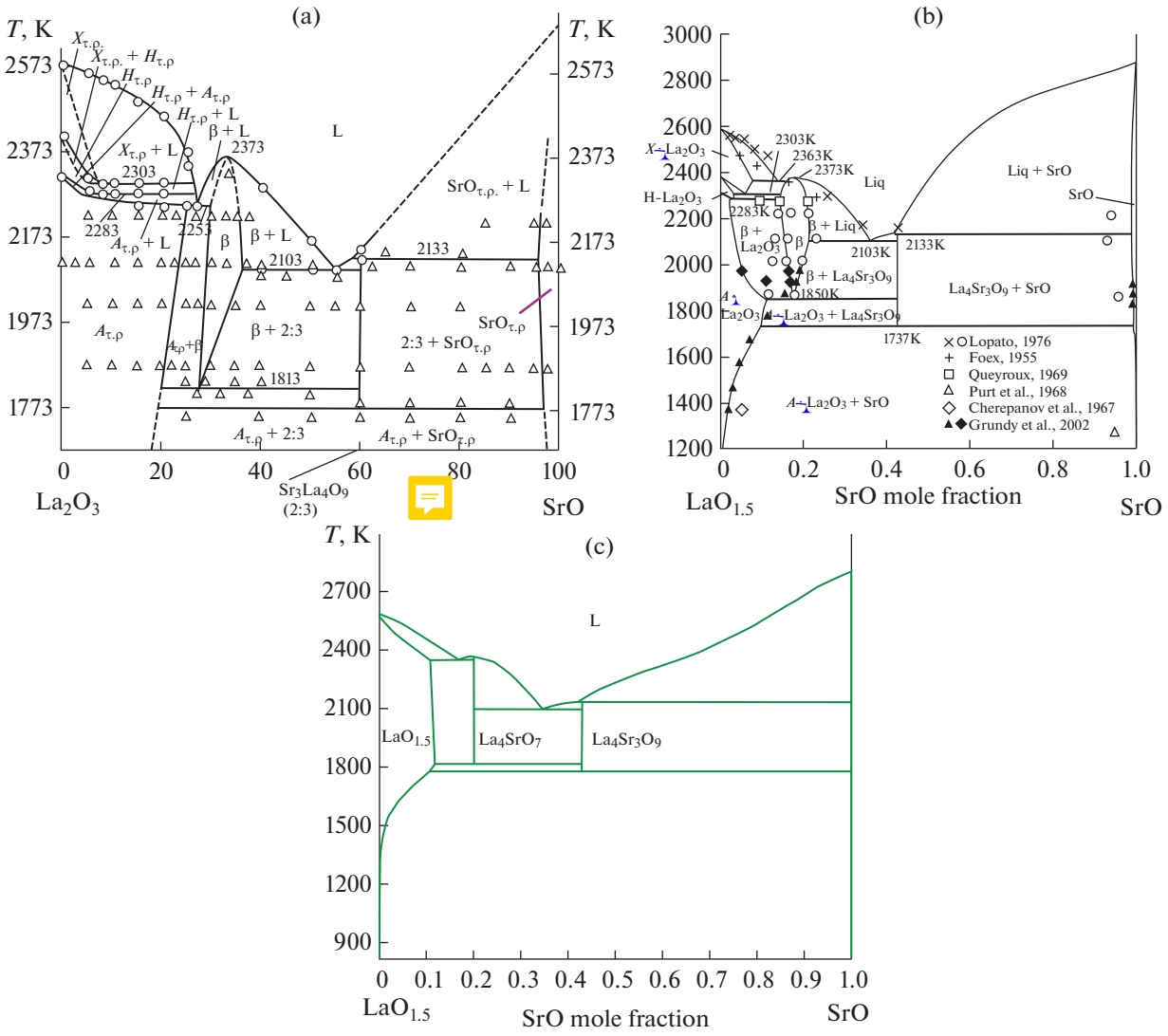

Fig. 1. La_2O_3–SrO phase diagram reproduced by courtesy of (a) Lopato [34], (b) Grundy et al. [35], and (c) the NUCLEA database [25].

these compounds as compounds with a zero homogeneity ~~extent~~, which contradicts previously published studies.

The La_2O_3–ZrO_2 phase diagram has been studied repeatedly [41, 42] (Fig. 2). The existence of an intermediate compound in the La_2O_3–ZrO_2 system, which is lanthanum zirconate $La_2Zr_2O_7$ with the pyrochlore structure and a homogeneity ~~extent~~ of 28–41 mol % La_2O_3, was found experimentally [41]. $La_2Zr_2O_7$ melts congruently at 2560 K. A noticeable solubility of ZrO_2 in La_2O_3 polymorphs and of La_2O_3 in fluorite cubic zirconium oxide (more than 20 mol % La_2O_3) was observed. The La_2O_3 solubility in tetragonal ZrO_2 does not exceed 3 mol % [41]. A cubic solid solution was observed in the concentration range between $La_2Zr_2O_7$ and La_2O_3 at temperatures above 2223 K; this solution was referred to as a bixbyite La_2O_3-~~base~~ solid solution [41], although this structure is known only for those ~~lanthanide~~ oxides that are in the ~~lanthanide~~ series after promethium~~,~~ and not for La_2O_3 [43].

The experimental study of the phase diagram of the La_2O_3–ZrO_2 phase diagram with subsequent optimization by the CALPHAD ~~method~~, found in Wang et al.'s paper [42] and reproduced in Fig. 2b, confirmed the formation of pyrochlore $La_2Zr_2O_7$ having a far narrower homogeneity ~~extent~~ of 31.8–34.6 mol % La_2O_3 and melting at 2556 K. The solubility of La_2O_3 in cubic ZrO_2 did not exceed 20 mol %, and in tetragonal zirconium dioxide it was less than 1 mol %. The ~~homogeneity region~~ in the concentration range between $La_2Zr_2O_7$ and La_2O_3 has the fluorite ZrO_2 structure, as Wang et al. believed [42]. More recent studies of phase equilibria in the Al_2O_3–La_2O_3–ZrO_2 system [44] showed that, for the best fit of the opti-

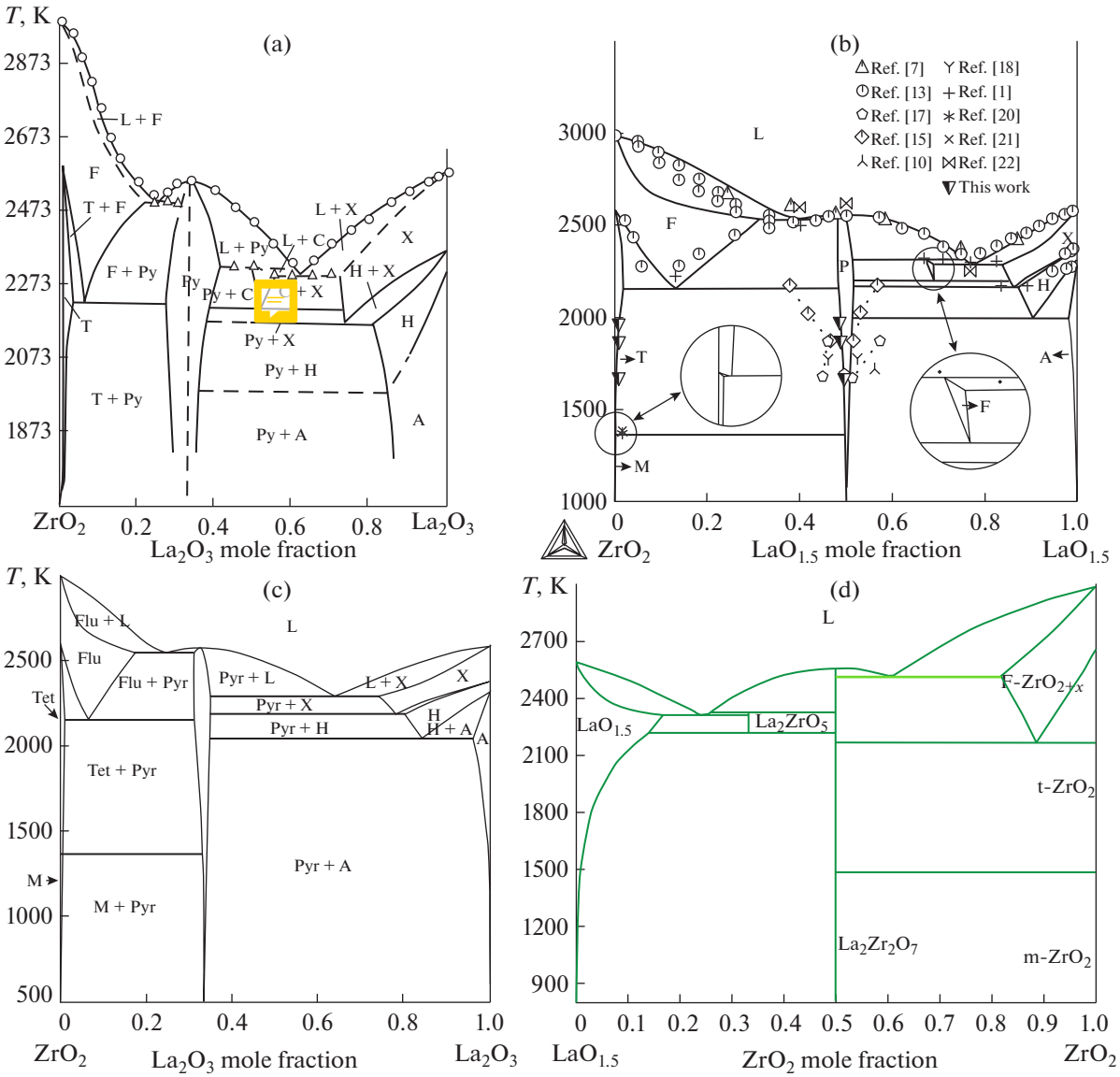

Fig. 2. La_2O_3–ZrO_2 phase diagram reproduced by courtesy of (a) Andrievskaya [41], (b) Wang et al. [42], (c) Fabrichnaya et al. [44], and (d) the NUCLEA database [25].

mized description of binary and ternary systems, it is advisable to abandon the idea of the homogeneity region in the concentration range between $La_2Zr_2O_7$ and La_2O_3, replacing it with equilibrium between $La_2Zr_2O_7$- and La_2O_3-base solid solutions (Fig. 2c).

The NUCLEA database uses older experimental results [45] for the optimization of phase equilibria in the La_2O_3–ZrO_2 system. Modeling of the phase diagram of the system under consideration in the NUCLEA database (Fig. 2d) gave the following results: the existence of lanthanum zirconate melting congruently at 2554 K; dissolution of ZrO_2 in La_2O_3, which is considered to have only one polymorph, to form a solid solution in the range 71.2–100.0 mol % La_2O_3; and dissolution of La_2O_3 only in cubic ZrO_2 up to 10.1 mol % La_2O_3. Instead of the homogeneity region in the concentration range between $La_2Zr_2O_7$ and La_2O_3 noted in [41, 42], the NUCLEA database assumes the formation of the compound La_2ZrO_5 with a zero homogeneity extent. Therefore, inconsistencies may arise between the phase equilibria in the La_2O_3–SrO–ZrO_2 system calculated using the NUCLEA database and by more advanced approaches as regards the $La_2Zr_2O_7$ and La_2ZrO_5 homogeneity regions, La_2O_3 solubility in tetragonal ZrO_2, and the existence of La_2O_3 polymorphs.

Phase relations in the SrO–ZrO_2 system were studied [46–49]. There is disagreement about the number of compounds formed in this system. Traverse and

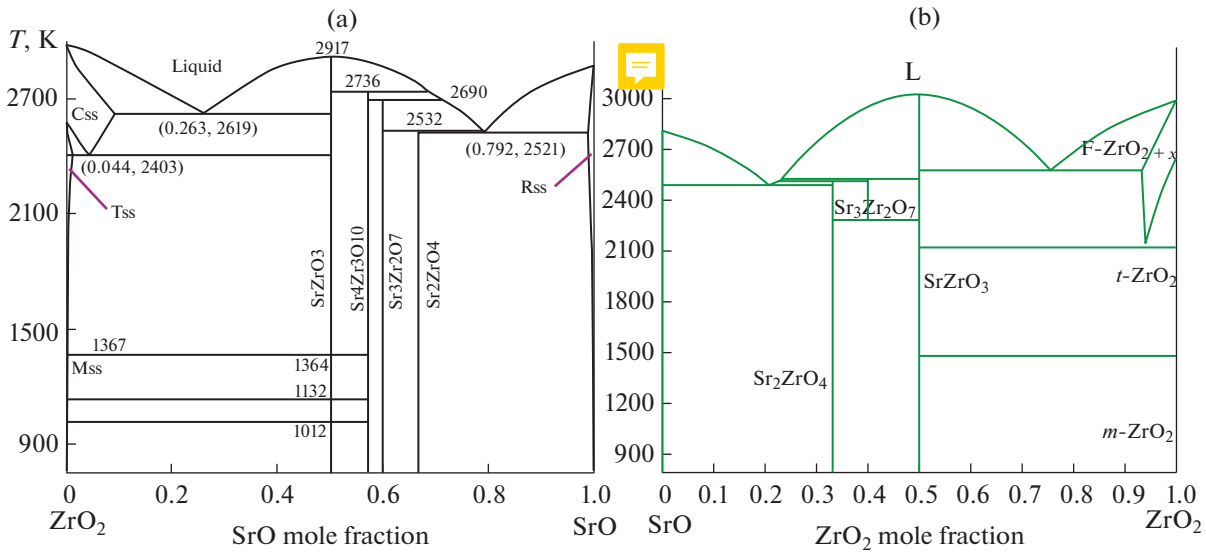

Fig. 3. SrO–ZrO_2 phase diagram reproduced by courtesy of (a) Gong et al. [49] and (b) the NUCLEA database ~~NUCLEA~~ [25].

Foex [46] found three intermediate compounds: $SrZrO_3$, Sr_2ZrO_4, and $Sr_3Zr_2O_7$; the last two melted incongruently, while $SrZrO_3$ melted congruently at 3023 K. The existence of four compounds in this system was also documented: $SrZrO_3$, Sr_2ZrO_4, $Sr_3Zr_2O_7$, and $Sr_4Zr_3O_{10}$ [47–49]. Gong et al. [49], along with experimentally studying phase equilibria, made optimization in terms of the CALPHAD approach. They showed that $SrZrO_3$ melts congruently at 2917 K, while Sr_2ZrO_4, $Sr_3Zr_2O_7$, and $Sr_4Zr_3O_{10}$ melt incongruently at 2532, 2690, and 2736 K, respectively (Fig. 3a). The optimization of phase equilibria in the SrO–ZrO_2 system in NUCLEA was according to experimental data obtained by Traverse and Foex [46] and by Noguchi et al. [47], taking into account only three compounds, as in [46] (Fig. 3b). According to NUCLEA, $Sr_3Zr_2O_7$ is formed at 2289 K by the reaction between $SrZrO_3$ and Sr_2ZrO_4, as opposed to Gong et al. [49], who ~~proved~~ the stability of $Sr_3Zr_2O_7$ at lower temperatures ~~experimentally~~. In NUCLEA, Sr_2ZrO_4 and $Sr_3Zr_2O_7$ melt incongruently at 2507 and 2521 K, respectively. The congruent melting temperature of $SrZrO_3$ is 3023 K. Thus, the SrO–ZrO_2 phase diagram modeled in NUCLEA differs significantly from Gong et al.'s most reliable work [49] both in the number of compounds formed in the system and in the $Sr_3Zr_2O_7$ formation temperature and melting temperatures.

No documents concerning phase equilibria in the La_2O_3–SrO–ZrO_2 ternary system have been found, which emphasizes the novelty of our work. As noted above, the limitations of the pioneering calculations carried out in this work using the NUCLEA database may include:

— Only one La_2O_3 polymorph is considered;

— The components are not dissolved in SrO and in tetragonal ZrO_2;

— The homogeneity regions in the La_2O_3–SrO and La_2O_3–ZrO_2 ~~system~~ are considered as the stoichiometric compounds La_4SrO_7 and La_2ZrO_5;

— Pyrochlore $La_2Zr_2O_7$-~~base~~ solid solution does not exist;

— One of the compounds ($Sr_4Zr_3O_{10}$) in the SrO–ZrO_2 system does not exist; and

— There are errors in optimization of the liquidus in the SrO–ZrO_2 system and in the temperature range of existence of the compound $Sr_3Zr_2O_7$.

To solve these and other problems of the computational study of the La_2O_3–SrO–ZrO_2 phase diagram, it would be advisable in the future to carry out a new study, both experimentally and using databases and software that would allow users to change and update data.

RESULTS AND DISCUSSION

First, let us dwell on isothermal sections of the La_2O_3–SrO–ZrO_2 phase diagram calculated using the NUCLEA database [25, 26] at increasing temperature and a constant external pressure equal to 1 atm. At temperatures below 646 K, four three-phase equilibria involving phases of constant composition were observed in the isothermal sections of the phase diagram: La_2O_3 + SrO + Sr_2ZrO_4, La_2O_3 + $La_2Zr_2O_7$ + Sr_2ZrO_4, $La_2Zr_2O_7$ + $SrZrO_3$ + Sr_2ZrO_4, and $La_2Zr_2O_7$ + $SrZrO_3$ + *m*-ZrO_2 (Fig. 4a), where *m*-ZrO_2 is monoclinic zirconium oxide. At 646 K, two three-phase equilibria change: instead of La_2O_3 + $La_2Zr_2O_7$ + Sr_2ZrO_4 and $La_2Zr_2O_7$ + $SrZrO_3$ +

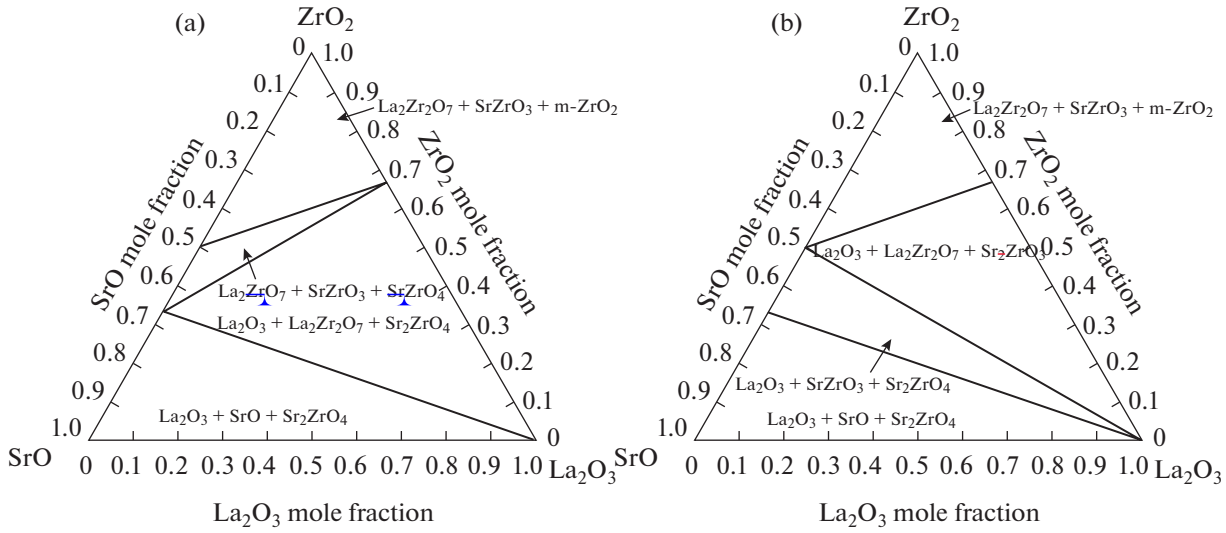

Fig. 4. Isothermal sections of the La_2O_3–SrO–ZrO_2 phase diagram calculated in this work using the NUCLEA database [25] (a) up to 646 K and (b) at 647 K.

Sr_2ZrO_4, the isothermal section features equilibria La_2O_3 + $SrZrO_3$ + Sr_2ZrO_4 and La_2O_3 + $La_2Zr_2O_7$ + $SrZrO_3$ (Fig. 4b). Consequently, up to 646 K, there was a two-phase equilibrium involving lanthanum pyrozirconate and strontium orthozirconate, which disappeared as temperature increased ~~to make place to~~ two-phase equilibrium involving lanthanum oxide and strontium metazirconate, which was not observed at lower temperatures. This evolution of phase equilibria may be called a quasi-peritectoid rearrangement,

$$La_2Zr_2O_7 + 2Sr_2ZrO_4 = La_2O_3 + 4SrZrO_3, \quad (1)$$

in which the $La_2Zr_2O_7$–Sr_2ZrO_4 stable diagonal changes to La_2O_3–$SrZrO_3$ as temperature rises. Similar quasi-peritectoid rearrangement was discovered earlier [19, 30] when the phase diagram of the Al_2O_3–SiO_2–ZrO_2 system at 1328.54 K was calculated using the NUCLEA database. It may be assumed that the discussed change in phase equilibria is not a property of the system under study~~,~~ but a calculation error. As mentioned above in the section "Calculation Methods", the calculation of phase equilibria in the CALPHAD approach is based on the optimized dependences of the Gibbs energies of all phases formed in the system. Phase relations and thermodynamic properties in the systems under consideration, as a rule, have been determined at higher temperatures. Consequently, Gibbs energies are extrapolated to calculate the phase diagram at low temperatures, at which extrapolation errors in optimized temperature-dependent thermodynamic properties may appear due to the similarity of the Gibbs energies in various sets of phases.

As temperature increases further, the monoclinic zirconium oxide transforms to the tetragonal polymorph at 1478 K; the homogeneity region of the La_2O_3-base solid solution expands; and accordingly, the two-phase fields of lanthanum oxide and samarium zirconates also expand (Fig. 5a). At 1777 K, the compound $La_4Sr_3O_9$ is formed in the La_2O_3–SrO system. It is for this reason that, instead of one three-phase equilibrium La_2O_3 + SrO + Sr_2ZrO_4, two three-phase equilibria, namely, $La_4Sr_3O_9$ + SrO + Sr_2ZrO_4 and La_2O_3 + $La_4Sr_3O_9$ + Sr_2ZrO_4, appear on the calculated ~~1778 K~~ isothermal section of the La_2O_3–SrO–ZrO_2 phase diagram (Fig. 5b). In addition, the La_2O_3 + $La_2Zr_2O_7$ two-phase field emerges as the homogeneity ~~extent~~ of the La_2O_3-~~base~~ solid solution increases. That is why hereafter La_2O_3 will be understood as a lanthanum oxide-~~base~~ solid solution.

At 1813.5 K, the second compound (La_4SrO_7) is formed in the La_2O_3–SrO system. However, the calculated ~~1814 K~~ isothermal section of the La_2O_3–SrO–ZrO_2 phase diagram (Fig. 6a) does not feature this compound. This may be due to ~~calculation~~ errors in the minimum total Gibbs energy of the system when polynomial-fitted concentration- and temperature-dependent thermodynamic properties are used. At 1815 K, the formation of the compound La_4SrO_7 is manifested in the replacement of La_2O_3 + $La_4Sr_3O_9$ + Sr_2ZrO_4 equilibrium by La_4SrO_7 + $La_4Sr_3O_9$ + Sr_2ZrO_4 and La_2O_3 + La_4SrO_7 + Sr_2ZrO_4 three-phase equilibria, as shown in Fig. 6b.

The La_2O_3–SrO system has the lowest-temperature binary eutectic in the ternary system under consideration, corresponding to the ~~solidification~~ of two intermediate compounds (La_4SrO_7 and $La_4Sr_3O_9$) at 2096 K. The calculated ~~2100 K~~ isothermal section of the La_2O_3–SrO–ZrO_2 phase diagram (Fig. 7a) indicates that the ternary eutectic point should have a lower temperature. The first ternary eutectic in the

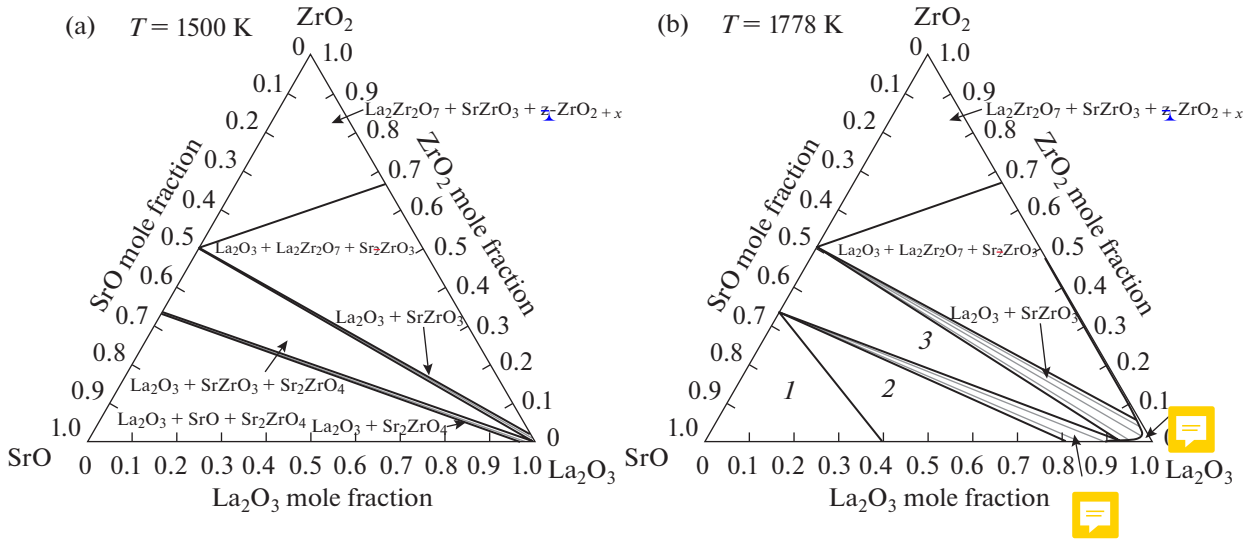

Fig. 5. Isothermal sections of the La_2O_3–SrO–ZrO_2 phase diagram calculated in this work using the NUCLEA database [25] at (a) 1500 and (b) 1778 K: (*1*) $La_4Sr_3O_9$ + SrO + Sr_2ZrO_4, (*2*) La_2O_3 + $La_4Sr_3O_9$ + Sr_2ZrO_4 and (*3*) La_2O_3 + $SrZrO_3$ + Sr_2ZrO_4. Gray lines correspond to tie-lines connecting the compositions of coexisting phases in two-phase equilibria.

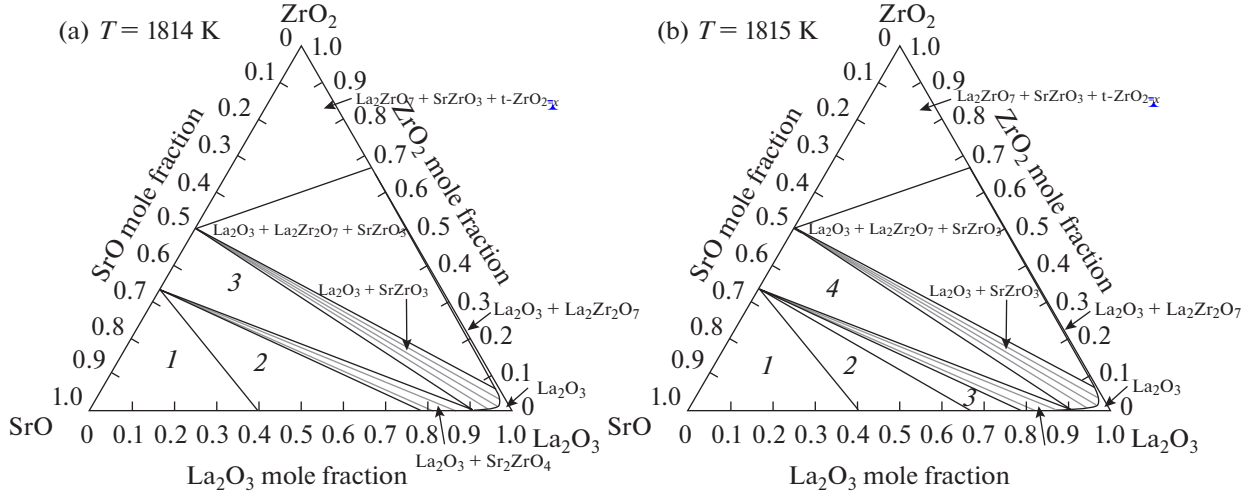

Fig. 6. Isothermal sections of the La_2O_3–SrO–ZrO_2 phase diagram calculated in this work using the NUCLEA database [25] (a) at 1814 K: (*1*) $La_4Sr_3O_9$ + SrO + Sr_2ZrO_4, (*2*) La_2O_3 + $La_4Sr_3O_9$ + Sr_2ZrO_4, and (*3*) La_2O_3 + $SrZrO_3$ + Sr_2ZrO_4; and (b) at 1815 K: (*1*) $La_4Sr_3O_9$ + SrO + Sr_2ZrO_4, (*2*) La_4SrO_7 + $La_4Sr_3O_9$ + Sr_2ZrO_4, (*3*) La_2O_3 + La_4SrO_7 + Sr_2ZrO_4, and (*4*) La_2O_3 + $SrZrO_3$ + Sr_2ZrO_4. Gray lines correspond to tie-lines connecting the compositions of coexisting phases in two-phase equilibria.

La_2O_3–SrO–ZrO_2 system appears at 2039 K, which is 57 K lower than the eutectic temperature in the binary system, and corresponds to four-phase equilibrium of La_4SrO_7, $La_4Sr_3O_9$, Sr_2ZrO_4, and the melt containing 44.9 mol % La_2O_3, 50.5 mol % SrO, and 4.6 mol % ZrO_2 (Table 1).

Figure 7a features a homogeneous melt area at 2100 K, two-phase and ~~melt-involving three-phase~~ fields numbered *1*–*9*, a homogeneous La_2O_3-~~base~~ solid solution field, and the phase fields involving ~~the~~ solid solution numbered *10*–13. Special attention should be paid to the homogeneous zirconium oxide-~~base~~ fluorite solid solution (F–ZrO_{2+x}) ~~field~~. According to the values optimized in NUCLEA, the transition between the tetragonal and fluorite phases in individual ZrO_2 occurs at 2650 K. However, strontium and lanthanum oxides help stabilize the fluorite solid solution F–ZrO_{2+x} at lower temperatures (below 2100 K). Fields *14*–*16* in Fig. 7a refer to equilibria involving F–ZrO_{2+x}.

The next section of the La_2O_3–SrO–ZrO_2 phase diagram shown in Fig. 7b was the ~~2132 K~~ section calculated ~~assuming~~ that the compound $La_4Sr_3O_9$ in the La_2O_3–SrO system melts incongruently at 2131 K. Indeed, Fig. 7b does not feature phase equilibria

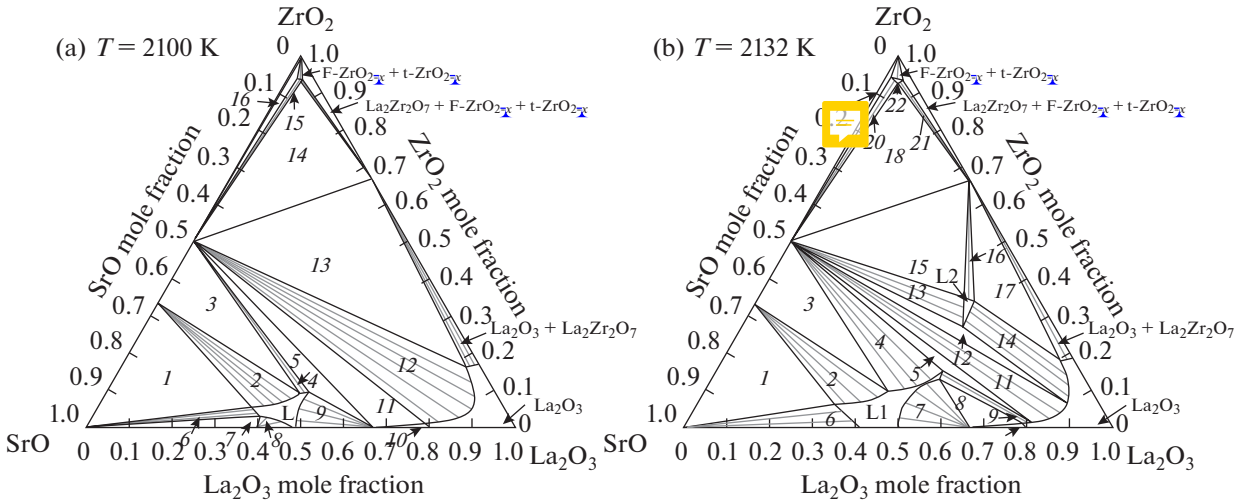

Fig. 7. Isothermal sections of the La_2O_3–SrO–ZrO_2 phase diagram calculated in this work using the NUCLEA database [25] at 2100 K (a): (*1*) L + SrO + Sr_2ZrO_4, (*2*) L + Sr_2ZrO_4, (*3*) L + $SrZrO_3$ + Sr_2ZrO_4, (*4*) L + $SrZrO_3$, (*5*) L + La_4SrO_7 + $SrZrO_3$, (*6*) L + SrO, (*7*) L + $La_4Sr_3O_9$ + SrO, (*8*) L + $La_4Sr_3O_9$, (*9*) L + La_4SrO_7, (*10*) La_2O_3 + La_4SrO_7, (*11*) La_2O_3 + La_4SrO_7 + $SrZrO_3$, (*12*) La_2O_3 + $SrZrO_3$, (*13*) La_2O_3 + $La_2Zr_2O_7$ + $SrZrO_3$, (*14*) $La_2Zr_2O_7$ + $SrZrO_3$ + F–ZrO_{2+x}, (*15*) $SrZrO_3$ + F–ZrO_{2+x}, and (*16*) $SrZrO_3$ + F–ZrO_{2+x} + *t*-ZrO_{2+x}; and (b) at 2132 K: (*1*) L1 + SrO + Sr_2ZrO_4, (*2*) L1 + Sr_2ZrO_4, (*3*) L1 + $SrZrO_3$ + Sr_2ZrO_4, (*4*) L1 + $SrZrO_3$, (*5*) L1 + La_2O_3 + $SrZrO_3$, (*6*) L1 + SrO, (*7*) L1 + La_4SrO_7, (*8*) L1 + La_2O_3 + La_4SrO_7, (*9*) L1 + La_2O_3, (*10*) La_2O_3 + La_4SrO_7, (*11*) La_2O_3 + $SrZrO_3$, (*12*) L2 + La_2O_3 + $SrZrO_3$, (*13*) L2 + $SrZrO_3$, (*14*) L2 + La_2O_3, (*15*) L2 + $La_2Zr_2O_7$ + $SrZrO_3$, (*16*) L2 + $La_2Zr_2O_7$, (*17*) L2 + La_2O_3 + $La_2Zr_2O_7$, (*18*) $La_2Zr_2O_7$ + $SrZrO_3$ + F–ZrO_{2+x}, (*19*) $SrZrO_3$ + F–ZrO_{2+x} + *t*-ZrO_{2+x}, (*20*) $SrZrO_3$ + F–ZrO_{2+x}, (*21*) $La_2Zr_2O_7$ + F–ZrO_{2+x}, and (*22*) F–ZrO_{2+x}. Gray lines correspond to tie-lines connecting the compositions of coexisting phases in two-phase equilibria.

involving $La_4Sr_3O_9$. A specific feature of the ~~2132 K~~ section is the appearance of a second homogeneous melt field, denoted in Fig. 7b as L2. Phase fields *1*–*9* refer to equilibria involving the first melt L1, and fields *12*–*17*, to equilibria involving L2.

The look of the ~~2132 K~~ isothermal section suggests the existence of two more eutectic points in the system under study. One eutectic corresponds to the homogeneous melt field L2, and the other is in the region ~~suspended~~ between the fields L1 + $SrZrO_3$ (field *4* in Fig. 7b), L1 + La_4SrO_7 (field *7*), and L1 + La_2O_3 (field *9*). Indeed, a more detailed consideration of phase equilibria in these regions makes it possible to identify invariant equilibria:

$$La_2O_3 + La_2Zr_2O_7 + SrZrO_3 \rightarrow L2 \qquad (2)$$

at 2105 K and a eutectic melt composition of 49.3 mol % La_2O_3, 17.0 mol % SrO, and 33.7 mol % ZrO_2; and

$$La_2O_3 + La_4SrO_7 + SrZrO_3 \rightarrow L1 \qquad (3)$$

at 2120 K and a melt composition of 52.4 mol % La_2O_3, 34.1 mol % SrO, and 13.5 mol % ZrO_2 (Table 1).

As temperature increases further, the compounds La_2ZrO_5 (T = 2208 K) and $Sr_3Zr_2O_7$ (T = 2289 K) are formed in the La_2O_3–ZrO_2 and SrO–ZrO_2 systems, respectively. The ~~2290 K~~ isothermal section of the La_2O_3–SrO–ZrO_2 phase diagram features phase equilibria involving these compounds: there are three fields involving La_2ZrO_5 (L + La_2ZrO_5 + $La_2Zr_2O_7$ (field *8*), L + La_2ZrO_5 (field *9*), and L + La_2O_3 + La_2ZrO_5 (field *10*) ~~in Fig. 8a~~) and two three-phase equilibria involving $Sr_3Zr_2O_7$ (L + Sr_2ZrO_4 + $Sr_3Zr_2O_7$ (field *3* in Fig. 8a) and L + $SrZrO_3$ + $Sr_3Zr_2O_7$ (field *4*) ~~in Fig. 8a~~). There is one more feature: melt fields L1 and L2, marked in Fig. 7, are here united into one single-phase area extending from the La_2O_3–SrO binary system to the maximum ZrO_2 percentage, equal to 45.7 mol %. In addition, there are no equilibria with the melt at 2290 K in the concentration areas unless

Table 1. Eutectic point coordinates in the La_2O_3–SrO–ZrO_2 system calculated using the NUCLEA database

Equilibrium	T, K	~~In melt~~, mol %		
		La_2O_3	SrO	ZrO_2
$La_4SrO_7 + La_4Sr_3O_9 + Sr_2ZrO_4 \rightarrow L$	2039	44.9	50.5	4.6
$La_2O_3 + La_2Zr_2O_7 + SrZrO_3 \rightarrow L$	2105	49.3	17.0	33.7
$La_2O_3 + La_4SrO_7 + SrZrO_3 \rightarrow L$	2120	52.4	34.1	13.5
$La_2Zr_2O_7 + SrZrO_3 + F–ZrO_{2+x} \rightarrow L$	2351	15.7	14.8	69.5

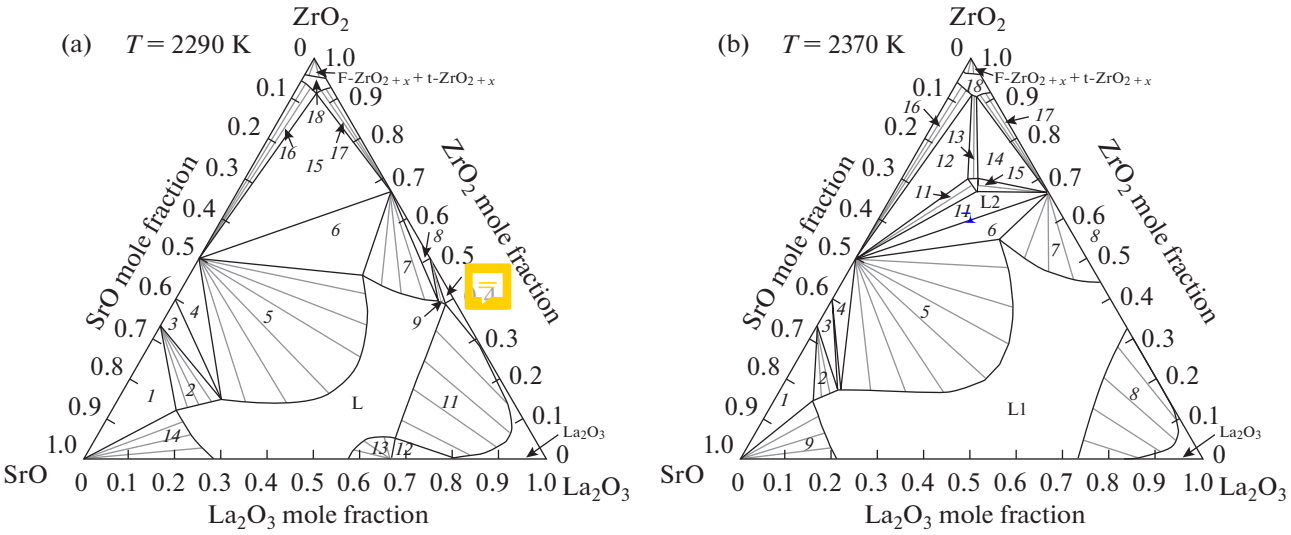

Fig. 8. Isothermal sections of the La_2O_3–SrO–ZrO_2 phase diagram calculated in this work using the NUCLEA database [25] (a) at 2290 K: (*1*) L + SrO + Sr_2ZrO_4, (*2*) L + Sr_2ZrO_4, (*3*) L + Sr_2ZrO_4 + $Sr_3Zr_2O_7$, (*4*) L + $SrZrO_3$ + $Sr_3Zr_2O_7$, (*5*) L + $SrZrO_3$, (*6*) L + $La_2Zr_2O_7$ + $SrZrO_3$, (*7*) L + $La_2Zr_2O_7$, (*8*) L + La_2ZrO_5 + $La_2Zr_2O_7$, (*9*) L + La_2ZrO_5, (*10*) L + La_2O_3 + La_2ZrO_5, (*11*) L + La_2O_3, (*12*) L + La_2O_3 + La_4SrO_7, (*13*) L + La_4SrO_7, (*14*) L + SrO, (*15*) $La_2Zr_2O_7$ + $SrZrO_3$ + F–ZrO_{2+x}, (*16*) $SrZrO_3$ + F–ZrO_{2+x}, (*17*) $La_2Zr_2O_7$ + F–ZrO_{2+x}, and (*18*) F–ZrO_{2+x}; and (b) at 2370 K: (*1*) L1 + SrO + Sr_2ZrO_4, (*2*) L1 + Sr_2ZrO_4, (*3*) L1 + Sr_2ZrO_4 + $Sr_3Zr_2O_7$, (*4*) L1 + $SrZrO_3$ + $Sr_3Zr_2O_7$, (*5*) L1 + $SrZrO_3$, (*6*) L1 + $La_2Zr_2O_7$ + $SrZrO_3$, (*7*) L1 + $La_2Zr_2O_7$, (*8*) L1 + La_2O_3, (*9*) L1 + SrO, (*10*) L2 + $La_2Zr_2O_7$ + $SrZrO_3$, (*11*) L2 + $SrZrO_3$, (*12*) L2 + $SrZrO_3$ + F–ZrO_{2+x}, (*13*) L2 + F–ZrO_{2+x}, (*14*) L2 + $La_2Zr_2O_7$ + F–ZrO_{2+x}, (*15*) L2 + $La_2Zr_2O_7$, (*16*) $SrZrO_3$ + F–ZrO_{2+x}, (*17*) $La_2Zr_2O_7$ + F–ZrO_{2+x}, and (*18*) F–ZrO_{2+x}. Gray lines correspond to tie-lines connecting the compositions of coexisting phases in two-phase equilibria.

the ZrO_2 percentage is lower than in the $La_2Zr_2O_7$–$SrZrO_3$ concentration section.

The ~~2370 K~~ isothermal section of the La_2O_3–SrO–ZrO_2 phase diagram has the following specific features: there is no equilibria involving La_2ZrO_5 or La_4SrO_7 because of them melting incongruently and congruently, respectively, at 2320 and 2370 K; the melt field contacts the La_2O_3–ZrO_2 binary system; and one more homogeneous melt field (L2) ~~with~~ emerges with the ZrO_2 ~~percentage~~ higher than along the $La_2Zr_2O_7$–$SrZrO_3$ concentration section. Homogeneous melt field L2 corresponds to the quaternary eutectic point $La_2Zr_2O_7$ + $SrZrO_3$ + F–ZrO_{2+x} → L2 in the system under consideration at 2351 K and a melt composition of 15.7 mol % La_2O_3, 14.8 mol % SrO, and 69.5 mol % ZrO_2 (Table 1). It is for the first time that a two-phase field of the fluorite ZrO_2-~~base~~ solid solution (F–ZrO_{2+x}) and melt appears on the calculated sections.

A further rise in temperature leads to sequential melting of phases in binary systems. The incongruent melting of Sr_2ZrO_4 and $Sr_3Zr_2O_7$ occurs ~~A~~t 2507 and 2521 K, respectively. For this reason, the ~~2522 K~~ section of the La_2O_3–SrO–ZrO_2 diagram does not feature phase equilibria involving these strontium zirconates (Fig. 9a). However, melt-involving two-phase equilibria survive with SrO (field *1* in Fig. 9a), $SrZrO_3$ (field *2*), F–ZrO_{2+x} (field *4*), $La_2Zr_2O_7$ (field *5*), and La_2O_3 (field *6*), as well as $SrZrO_3$ + F–ZrO_{2+x} ~~equilibria~~ (field *7*) and ~~equilibria~~ of cubic and tetragonal zirconium ~~oxide base solid solutions~~. Still further increase in temperature leads to melting of $La_2Zr_2O_7$ and the disappearance of L + $La_2Zr_2O_7$ equilibrium on the ~~2554 K~~ section (Fig. 9b). On the ~~2587 K~~ isothermal section of the La_2O_3–SrO–ZrO_2 phase diagram (Fig. 9c), in addition to the disappearance of the homogeneous La_2O_3 field and the L + La_2O_3 field because of lanthanum oxide melting at 2586 K, there are no three-phase fields and there is no $SrZrO_3$ + F–ZrO_{2+x} equilibrium because of the melt area touching the SrO–ZrO_2 binary system in the range from $SrZrO_3$ to ZrO_2. Thus, only two-phase equilibria with the melt exist at temperatures ~~below~~ 2587 K in the system under consideration; these are equilibria involving strontium oxide, strontium metazirconate, and the fluorite zirconium oxide-~~base~~ solid solution. In addition, stable are the F–ZrO_{2+x} homogeneous field and F–ZrO_{2+x} + *t*-ZrO_{2+x} two-phase equilibrium; the latter will exist until the individual tetragonal zirconium oxide transforms to the cubic phase at 2650 K.

In view of the importance of the compounds $La_2Zr_2O_7$ and $SrZrO_3$ in various fields of modern materials science [4, 8, 10], a polythermal section of the La_2O_3–SrO–ZrO_2 phase diagram was calculated for the $La_2Zr_2O_7$–$SrZrO_3$ concentration section, as shown in Fig. 10. This polythermal section belongs to the simplest eutectic type without solid solutions. Apparently, the absence of solid solutions in this poly-

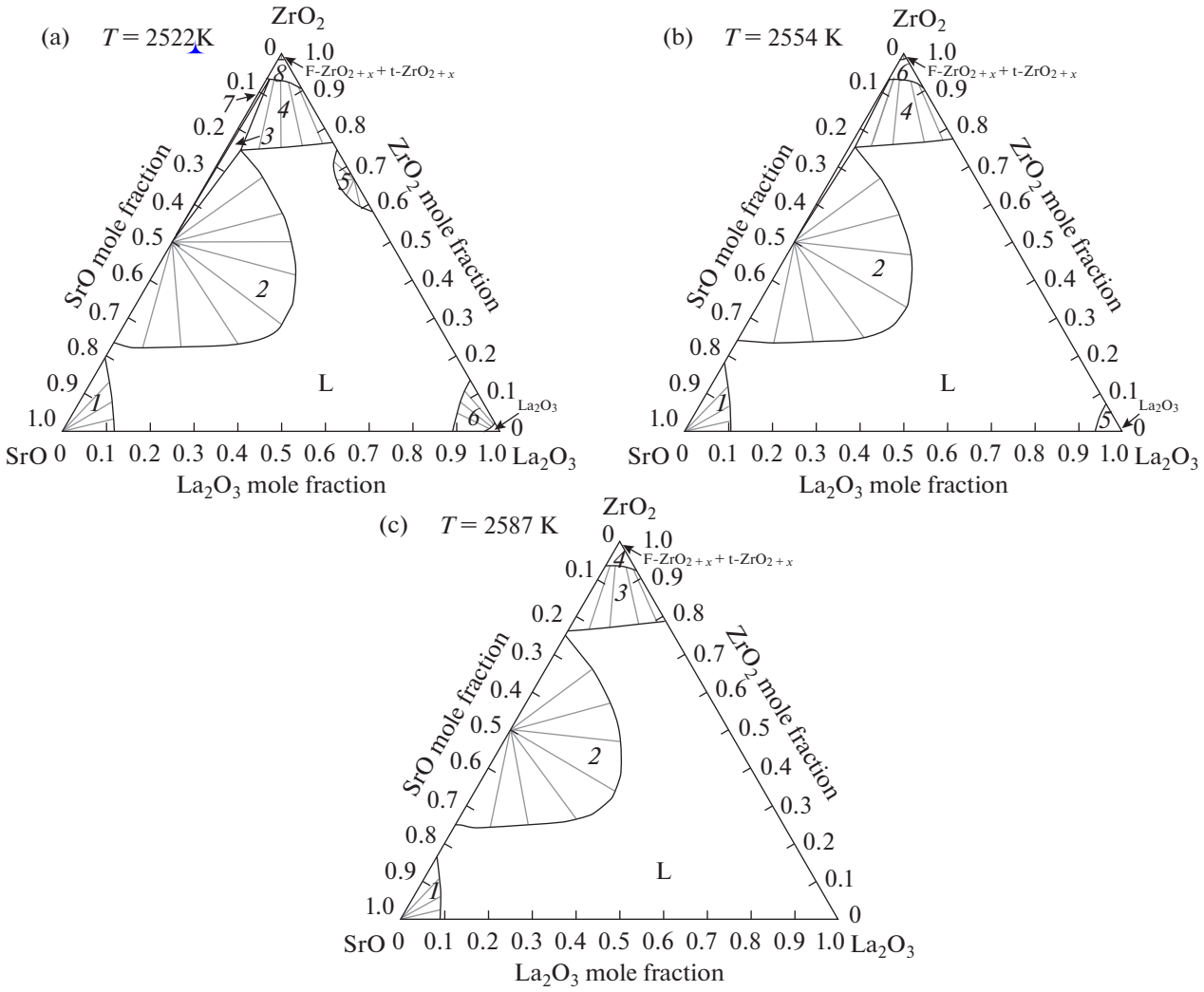

Fig. 9. Isothermal sections of the La_2O_3–SrO–ZrO_2 phase diagram calculated in this work using the NUCLEA database [25] at (a) 2522 K: (*1*) L + SrO, (*2*) L + $SrZrO_3$, (*3*) L + $SrZrO_3$ + F–ZrO_{2+x}, (*4*) L + F–ZrO_{2+x}, (*5*) L + $La_2Zr_2O_7$, (*6*) L + La_2O_3, (*7*) $SrZrO_3$ + F–ZrO_{2+x}, and (*8*) F–ZrO_{2+x}; (b) at 2554 K: (*1*) L + SrO, (*2*) L + $SrZrO_3$, (*3*) L + $SrZrO_3$ + F–ZrO_{2+x}, (*4*) L + F–ZrO_{2+x}, (*5*) L + La_2O_3, and (*6*) F–ZrO_{2+x}; and (c) at 2587 K: (*1*) L + SrO, (*2*) L + $SrZrO_3$, (*3*) L + F–ZrO_{2+x}, and (*4*) F–ZrO_{2+x}. Gray lines correspond to tie-lines connecting the compositions of coexisting phases in two-phase equilibria.

thermal section, at least on the side of lanthanum pyrozirconate, flows from the assumption adopted in the NUCLEA database about the zero homogeneity regions of intermediate compounds in the La_2O_3–ZrO_2 and SrO–ZrO_2 binary systems, while according to more recent literature data described in the "Calculation Methods" section, lanthanum pyrozirconate has a nonzero homogeneity region and can form solid solutions. For this reason, the determination of strontium oxide solubility in $La_2Zr_2O_7$ is an interesting scientific problem for future experimental studies.

The $La_2Zr_2O_7$–$SrZrO_3$ section calculated in this work (Fig. 10) is a quasi-binary section; that is, the compositions of all phases involved in two-phase equilibria lie on this section, and there are no fields of three-phase equilibria over the entire range of temperatures studied. Therefore, the point in Fig. 10 that corresponds to equilibrium $La_2Zr_2O_7 + SrZrO_3 \rightarrow L$ at 2387 K and a melt composition of 22.8 mol % La_2O_3, 15.8 mol % SrO, and 61.4 mol % ZrO_2, is a eutectic point in the $La_2Zr_2O_7$–$SrZrO_3$ quasi-binary system and an analogue of a saddle point in the La_2O_3–SrO–ZrO_2 ternary system, i.e., a point with the highest liquidus temperature on the primary crystallization path between the second and fourth eutectics from Table 1 and with the lowest liquidus temperature on the path between $La_2Zr_2O_7$ and $SrZrO_3$ (Fig. 10). This becomes more obvious if we consider Fig. 8b, from which it flows that the eutectic is formed in the $La_2Zr_2O_7$–$SrZrO_3$ quasi-binary system when homogeneous melt fields L1 and L2 come in contact on the $La_2Zr_2O_7$–$SrZrO_3$ concentration section, and L1 + $La_2Zr_2O_7$ +

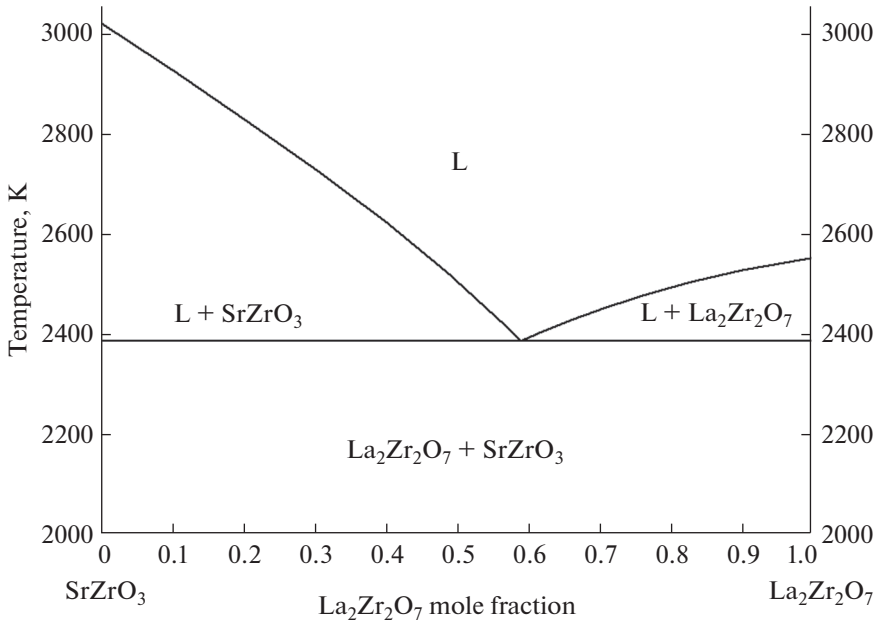

Fig. 10. Polythermal section $La_2Zr_2O_7$–$SrZrO_3$ of the La_2O_3–SrO–ZrO_2 phase diagram calculated in this work using the NUCLEA database [25].

$SrZrO_3$ (field *6*) and L2 + $La_2Zr_2O_7$ + $SrZrO_3$ (field *10*) equilibria disappear.

CONCLUSIONS

In this work, the phase diagram of the La_2O_3–SrO–ZrO_2 system has been studied by calculating fourteen sections using the NUCLEA database [25, 26]. No information has been retrieved in the literature on phase equilibria in the La_2O_3–SrO–ZrO_2 ternary system, so our results are the first attempt to study phase relations in this system, which is promising for a wide range of ~~relevant~~ applications in ~~advanced~~ materials science. The results of modeling of the La_2O_3–SrO–ZrO_2 phase diagram have been compared to available data on the constituent binary systems. Potential problems in the calculations have been identified, including those arising from the forbiddance to the user to make changes to the NUCLEA database in order to revise the initial data set used in the modeling and take into account the results of new studies of phase relations and thermodynamic properties. Therefore, it would be expedient in future to use the CALPHAD approach to consider phase equilibria in the La_2O_3–SrO–ZrO_2 system, with a mandatory preliminary experimental study of phase equilibria and thermodynamic properties in this ternary system at high temperatures.

FUNDING

This work was supported by the Russian Science Foundation (project No. 23-13-00254).

CONFLICT OF INTEREST

The authors declare that they have no conflicts of interest.

REFERENCES

1. A. Sarkar, R. Djenadic, D. Wang, et al., J. Eur. Ceram. Soc. **38**, 2318 (2018). https://doi.org/10.1016/j.jeurceramsoc.2017.12.058
2. D. A. Vinnik, E. A. Trofimov, V. E. Zhivulin, et al., Nanomaterials **10**, 268 (2020). https://doi.org/10.3390/NANO10020268
3. O. V. Zaitseva, S. A. Gudkova, E. A. Trofimov, et al., IOP Conf. Ser. Mater. Sci. Eng. **1014**, 012060 (2021). https://doi.org/10.1088/1757-899X/1014/1/012060
4. W. Ma, X.-L. Jin, Y. Ren, et al., ITSC Proc. 867 (2015). https://doi.org/10.31399/asm.cp.itsc2015p0867
5. L. Nalbandian, A. Evdou, and V. Zaspalis, Int. J. Hydrogen Energy **36**, 6657 (2011). https://doi.org/10.1016/j.ijhydene.2011.02.146
6. M. Keller, D. P. Anderson, H. Leion, et al., Appl. Catal., A: Gen. **550**, 105 (2018). https://doi.org/10.1016/j.apcata.2017.10.020
7. A. Klimkowicz, K. Świerczek, A. Takasaki, et al., Solid State Ionics **257**, 23 (2014). https://doi.org/10.1016/j.ssi.2014.01.018
8. S. A. Speakman, R. D. Carneim, E. A. Payzant, et al., J. Mater. Eng. Perform. **13**, 303 (2004). https://doi.org/10.1361/10599490419270
9. J. Dąbrowa, A. Olszewska, A. Falkenstein, et al., J. Mater. Chem. A **8**, 24455 (2020). https://doi.org/10.1039/d0ta06356h
10. E. Antonova, E. Tropin, and A. Khodimchuk, Ionics **28**, 5181 (2022). https://doi.org/10.1007/s11581-022-04750-w

11. J. Yan, D. Wang, X. Zhang, et al., J. Mater. Sci. **55**, 6942 (2020). https://doi.org/10.1007/s10853-020-04482-0
12. V. A. Shestakov and E. V. Grachev, Russ. J. Inorg. Chem. **67**, 488 (2022). https://doi.org/10.1134/S0036023622040179
13. V. A. Vorozhtcov and V. L. Stolyarova, Tech. Phys. **66**, 872 (2021). https://doi.org/10.1134/S1063784221060219
14. V. I. Lutsyk and A. E. Zelenaya, Russ. J. Inorg. Chem. **63**, 966 (2018). https://doi.org/10.1134/S0036023618070148
15. V. I. Lutsyk and A. E. Zelenaya, Russ. J. Inorg. Chem. **63**, 1087 (2018). https://doi.org/10.1134/S0036023618080132
16. V. P. Vorob'eva, A. E. Zelenaya, V. I. Lutsyk, et al., Glass Phys. Chem. **47**, 616 (2021). https://doi.org/10.1134/S1087659621060328
17. V. P. Vorob'eva, A. E. Zelenaya, and V. I. Lutsyk, Russ. J. Inorg. Chem. **66**, 894 (2021). https://doi.org/10.1134/S003602362106022X
18. M. Hillert, Int. Met. Rev. **30**, 45 (1985). https://doi.org/10.1179/imtr.1985.30.1.45
19. V. Vorob'eva, A. Zelenaya, V. Lutsyk, et al., Mater. Sci. Eng. **297**, 116790 (2023). https://doi.org/10.1016/J.MSEB.2023.116790
20. N. Saunders and A. P. Miodownik, www.elsevier.com/books/calphad-calculation-of-phase-diagrams-a-comprehensive-guide/saunders/978-0-08-042129-2 (accessed May 14, 2020)
21. H. L. Lukas, S. G. Fries, and B. Sundman, *Computational Thermodynamics: The Calphad Method* (Cambridge University Press, New York, 2007). https://doi.org/10.1017/CBO9780511804137
22. J. O. Andersson, T. Helander, L. Höglund, et al., Calphad Comput. Coupling Phase Diagrams Thermochem. **26**, 273 (2002). https://doi.org/10.1016/S0364-5916(02)00037-8
23. R. H. Davies, A. T. Dinsdale, J. A. Gisby, et al., Calphad Comput. Coupling Phase Diagrams Thermochem. **26**, 229 (2002). https://doi.org/10.1016/S0364-5916(02)00036-6
24. C. W. Bale, P. Chartrand, S. A. Degterov, et al., Calphad Comput. Coupling Phase Diagrams Thermochem. **26**, 189 (2002). https://doi.org/10.1016/S0364-5916(02)00035-4
25. S. Bakardjieva, M. Barrachin, S. Bechta, et al., Prog. Nucl. Energy **52**, 84 (2010). https://doi.org/10.1016/j.pnucene.2009.09.014
26. NUCLEA: Thermodynamic database for nuclear applications [~~Электронный ресурс~~]. URL: http://thermodata.online.fr/nuclea.html (~~дата обращения 30.03.2020~~).
27. C. Guéneau, N. Dupin, L. Kjellqvist, et al., CALPHAD: Comput. Coupling Phase Diagrams Thermochem. **72**, 102212 (2021). https://doi.org/10.1016/j.calphad.2020.102212
28. V. L. Stolyarova, Russ. Chem. Rev. **85**, 60 (2016). https://doi.org/10.1070/RCR4549
29. S. V. Bechta, V. S. Granovsky, V. B. Khabensky, et al., Nucl. Eng. Des. **238**, 2761 (2008). https://doi.org/10.1016/J.NUCENGDES.2008.04.018
30. V. A. Vorozhtcov, D. A. Yurchenko, V. I. Almjashev, et al., Glass Phys. Chem. **47**, 417 (2021). https://doi.org/10.1134/S1087659621050175
31. V. A. ~~Vorozhtsov~~, V. I. ~~Al'myashev~~, and V. L. Stolyarova, *Proceedings of the Symposium with international participation "Thermodynamics and Materials Science," Novosibirsk, Russia, 2023*, p. 76. https://doi.org/10.26902/THERM_2023_056
32. B. Sundman and J. Ågren, J. Phys. Chem. Solids **42**, 297 (1981). https://doi.org/10.1016/0022-3697(81)90144-X
33. O. Redlich and A. T. Kister, Ind. Eng. Chem. **40**, 345 (1948). https://doi.org/10.1021/ie50458a036
34. L. M. Lopato, Ceramurg. Int. **2**, 18 (1976). https://doi.org/10.1016/0390-5519(76)90004-1
35. A. N. Grundy, B. Hallstedt, and L. J. Gauckler, Acta Mater. **50**, 2209 (2002). https://doi.org/10.1016/S1359-6454(01)00432-3
36. H. Kitaguchi, M. Ohno, M. Kaichi, et al., J. Ceram. Soc. Jpn. **96**, 397 (1988). https://doi.org/10.2109/jcersj.96.397
37. L. Y. Gavrilova, T. V. Aksenova, and V. A. Cherepanov, Russ. J. Inorg. Chem. **53**, 953 (2008). https://doi.org/10.1134/S0036023608060235
38. W.-W. Zhang, E. Povoden-Karadeniz, Y. Shang, et al., J. Eur. Ceram. Soc. **43**, 4419 (2023). https://doi.org/10.1016/j.jeurceramsoc.2023.03.026
39. A.-R. Schulze and H. Müller-Buschbaum, Z. Anorg. Allg. Chem. **471**, 59 (1980). https://doi.org/10.1002/zaac.19804710106
40. Z. K. Huang, D. S. Yan, T. Y. Tien, et al., Mater. Lett. **11**, 286 (1991). https://doi.org/10.1016/0167-577X(91)90204-J
41. E. R. Andrievskaya, J. Eur. Ceram. Soc. **28**, 2363 (2008). https://doi.org/10.1016/j.jeurceramsoc.2008.01.009
42. C. Wang, O. Fabrichnaya, M. Zinkevich, et al., Calphad Comput. Coupling Phase Diagrams Thermochem. **32**, 111 (2008). https://doi.org/10.1016/j.calphad.2007.07.005
43. M. Zinkevich, Prog. Mater. Sci. **52**, 597 (2007). https://doi.org/10.1016/J.PMATSCI.2006.09.002
44. O. Fabrichnaya, S. Lakiza, C. Wang, et al., J. Alloys Compd. **453**, 271 (2008). https://doi.org/10.1016/j.jallcom.2006.11.102
45. A. Rouanet, Rev. Int. Hautes Temp. Refract. **8**, 161 (1971).
46. J. P. Traverse and M. Foex, High Temp. - High Press. **1**, 409 (1969).
47. T. Noguchi, T. Okubo, and O. Yonemochi, J. Am. Ceram. Soc. **52**, 178 (1969). https://doi.org/10.1111/J.1151-2916.1969.TB13360.X
48. S. Dash, D. D. Sood, and R. Prasad, J. Nucl. Mater. **228**, 83 (1996). https://doi.org/10.1016/0022-3115(95)00199-9
49. W. Gong, Y. Xie, Z. Zhao, et al., J. Am. Ceram. Soc. **103**, 1425 (2020). https://doi.org/10.1111/jace.16812

Translated by O. Fedorova

SPELL: 1. дата, 2. обращения